THE EFFECTS OF LAND COVER CHANGES ON LAND SURFACE TEMPERATURES

N. Aslan [1], D. Koc-San [2] *
[1] Akdeniz University, Faculty of Science, Dept. of Space Sciences and Technologies, Antalya, Türkiye - nagihanaslan@akdeniz.edu.tr
[2] Akdeniz University, Faculty of Architecture, Dept. of Urban and Regional Planning, Antalya, Türkiye - dkocsan@akdeniz.edu.tr

KEY WORDS: Land Cover Mapping, Land Surface Temperature, Change Detection, Greenhouse, Land Cover Indices

ABSTRACT:

The aims of this study are to detect the land-cover maps and land surface temperatures using Landsat time series and analyse the relation between the land-cover and land surface temperatures (LST) and their changes in time. For these purposes initially, land-cover maps were generated rapidly using land cover indices and automatic thresholding. The land-cover indices used in this study are Normalized Difference Vegetation Index (NDVI), Modified Normalized Difference Water Index (MNDWI), Index-Based Built-Up Index (IBI), Modified Bare-Soil Index (MBI), Plastic-Mulched Landcover Index (PMLI), Plastic Greenhouse Index (PGI) and Normalized Burn Ratio Thermal (NBRT) Index. Then, using the thermal bands of Landsat satellites, LST maps were created. Finally, the land-cover and LST changes were examined. The Kumluca district of Antalya, which includes extensive greenhouse areas as well as urban, vegetation, bareland, water, was selected as study area. Between the years 2004 and 2021, within the study area the greenhouse areas increased significantly, the urban area expanded and some areas exposed to fire, especially the fire in 2016. Therefore, the images within this time period were used. The overall accuracies for land-cover maps were computed as 76%, 79%, 79%, 89% and 86% for the years 2004, 2009, 2013, 2017 and 2021, respectively. The results obtained from the study reveal that while greenhouse and urban areas were increased, the vegetation areas were decreased significantly within this time period. In addition, generally increases were observed for LST values of all land-cover classes and the highest LST values were detected for the burned, bareland, urban and greenhouse areas.

1. INTRODUCTION

With population growth, urbanization is increasing in the world and land covers are changing rapidly. For this reason, land cover change detection is an important research topic for many research areas. Using remote sensing data and methods is a fast and low-cost way to determine land cover pattern. There are studies that use various land cover indices for land cover detection (Chen et al., 2006; Estoque et al., 2017; Aslan and Koc-San, 2021). Normalized Difference Vegetation Index (NDVI), Normalized Difference Water Index (NDWI), Soil-Adjusted Vegetation Index (SAVI), Normalized Difference Built-up Index (NDBI) are frequently used indices for this purpose.

Plastic covered greenhouse areas have expanded rapidly around the world in the last 20 years and now represent a significant amount of cultivated land (Lu et al., 2014). Türkiye is among the first four countries in the world in terms of greenhouse areas, while in Europe ranks second after Spain. In Türkiye, the 48% of greenhouse production (about 3.8 million tons) is made in Antalya (Republic of Türkiye Ministry of Agriculture and Forestry, 2023). Kumluca district has dense greenhouse areas and the increase in greenhouse areas continues. Providing up-to-date greenhouse database and determining its effect on LST is important for yield estimation, sustainable development and management. Various indices have been developed to determine greenhouse areas such as Plastic-Mulched Land Cover Index (Lu et al., 2014), Plastic Greenhouse Index (Yang et al., 2017), Moment Distance Index (Salas and Henebry, 2012) and Greenhouse Detection Index (Gonzalez-Yebra et al., 2018). In most of the studies in the literature, generally a special land class (such as urban areas or greenhouse areas) was determined using an index.

In this study, we used different land cover indices and an automatic thresholding method to generate land cover maps. There are studies in the literature that analyse the relationship between Land Use/Land Cover (LULC) types and LST values. Tan et al. (2020) drew attention to that the temperature of water surfaces is lower than other areas in their study and suggested that the water body has a regulating effect on the LST and surface thermal effects at a certain distance around it, and the closer the land cover area to the water body, the lower the LST value. Nega and Balew (2022), in their systematic review of 100 studies in the last 5 years, stated that the urban areas and their neighbouring bare land have highest LST values among 13 LULC types. They also indicated that snow cover has the lowest LST values in 13 LULC areas and water bodies also have lower LSTs compared to vegetation areas. In addition, in this study, it was indicated that the most commonly used satellites to obtain LST are Landsat 8 OLI/TIRS and Landsat 5 TM. Sekertekin et al. (2016), using Landsat 5 and 8 sensor data, examined the LST changes in and around the Zonguldak industrial zone and stated that the land use density in city centers, industrial enterprises, coal dumping site and municipal dump and land cover changes in the power plants area caused the LST to increase in these regions. It has been found that especially the regions where industrial enterprises are located have high LST values. The highest LST values were also observed in the coal dump site and the municipal dump. Supervised/unsupervised or

* Corresponding author

object-based classification techniques, linear spectral mixture analysis or hybrid methods are generally used in studies examining the LULC (Pal and Ziaul, 2017; Singh et al., 2017, Mathew et al., 2017; Zhao et al., 2016). In addition to these techniques, indices are used to define LULC types (Chen et al., 2006; Estoque et al., 2017; Aslan and Koc-San, 2021). In these studies, the mostly analysed land cover classes were urban, rural, vegetation, and water areas. Chen et al. (2006) also determined built-up, bareland, vegetation, water, semi-bareland areas using manual threshold values. Estoque et al. (2017) have defined LULC types as, water, impervious surface, green space, and other areas by applying the threshold values that they usually determine manually (determined the threshold value for only water areas by Otsu's thresholding method) to various indices. Studies that determine land cover type with automatic threshold value generally concentrate on a single class. For example, Muzaky and Jaelani (2019), used the Otsu's thresholding method to determine only water areas from the MNDWI data, while Şekertekin and Zadbagher (2021) used this method to extract impervious areas from the NDBI images.

The main purposes of this study are to detect land cover and LST maps between the years 2004-2021 using Landsat satellite images, and to analyse the LST changes of land cover areas in time and how land cover changes affect the LST values. Kumluca district of Antalya, which is known as dense greenhouse areas, were selected as study area. For these purposes, firstly land cover maps were generated using the land cover indices. In this study, the land cover classes were determined as urban, vegetation, greenhouse, water, burned area and bareland areas. To determine these areas Normalized Difference Vegetation Index (NDVI), Modified Normalized Difference Water Index (MNDWI), Index-Based Built-Up Index (IBI), Modified Bare-Soil Index (MBI), Plastic-Mulched Landcover Index (PMLI), Plastic Greenhouse Index (PGI) and Normalized Burn Ratio Thermal (NBRT) Index were used. Land cover classes were determined by applying the automatically computed threshold values to the created indices. Then, LST images were generated using the thermal bands. Finally, the land cover changes in the determined time interval and the effects of these changes on LST values were analysed.

2. STUDY AREA AND DATA SETS

Kumluca district, which is located in the west of Antalya province of Türkiye, is selected as study area (Figure 1). The most important income source of the district is greenhouse agriculture and citrus production. In the Kumluca district, there has been an important increase in greenhouse areas, especially in recent decades. On the other hand, there are areas that were significantly affected by the fires, especially the fire in 2016. This district has been determined as the study area in order to examine the changes in land cover and land surface temperatures due to different reasons such as increase in greenhouse areas, fire and urban sprawl.

The Landsat satellite series has been providing remote sensing data since 1972. The data sets used in this study are Landsat 5 TM images for the years 2004 (11/10/2004) and 2009 (09/10/2009) and Landsat 8 OLI/TIRS images for the years 2013 (20/10/2013), 2017 (15/10/2017) and 2021 (10/10/2021). Various indices were used to determine the areas in the study. The Green, Red, NIR, SWIR and Thermal bands of Landsat data were used while computing these indices and determining LST images.

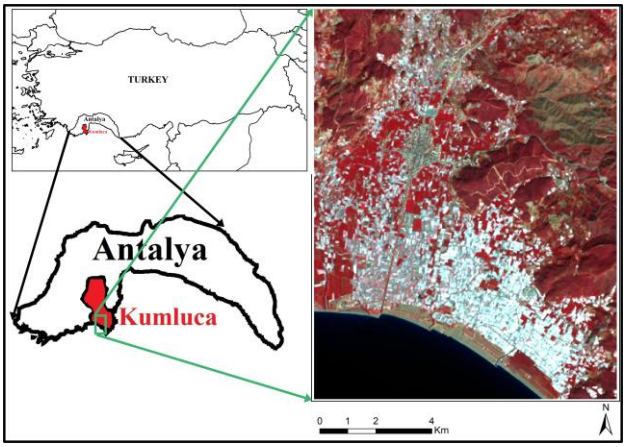

Figure 1. Location of Kumluca district in Antalya and Türkiye (left) and the colour infrared composite of study area (right).

3. METHODOLOGY

In this study, there are basically 3 steps, which are (i) Generation of land cover thematic maps, (ii) Generation of LST maps and (iii) Accuracy assessment of land cover classification and LST determination

3.1 Generation of Land Cover Thematic Maps

Different land cover classes can be detected using remote sensing indices (Estoque et al., 2017; Muzaky and Jaelani, 2019; Aslan and Koc-San, 2021). For example, NDVI contains essential information about vegetation in the areas. The MNDWI facilitate the detection of water areas, while IBI is used for detecting impervious or man-made surfaces. Due to the increasing food needs and climate changes, nowadays greenhouse production has become more necessary. The greenhouse indices are useful for determining the greenhouse areas rapidly and accurately. Studies are conducted on various indices that will facilitate the detection of greenhouses such as PMLI (Lu et al, 2014), PGI (Yang et al., 2017), Moment Distance Index (Salas and Henebry, 2012) and PGI (Gonzalez-Yebra et al, 2018). The study area was classified as urban, vegetation, greenhouse, water, burned and other areas, using land cover indices. In this study, in addition to NDVI, MNDWI, IBI, PMLI and PGI indices, the NBRT index was used to determine the burned areas and the MBI index was used to prevent mixing of urban, greenhouse and bare soil areas and to contribute to the accuracy of land cover classification (Table 1).

Firstly, by using Python programming language, atmospheric correction was applied to the multispectral bands to be used (USGS, 2021). Indices were created using the Python programming language (Figure 2). The Otsu's thresholding method (Otsu,1979) is widely used for automatic thresholding. There are two methods in the Python programming language that can be used to set one or more thresholds. Images were analysed and a single threshold value was calculated for the MNDWI, PMLI, and PGI indices, and double threshold values were calculated for the NDVI, IBI, MBI and NBRT indices by Otsu's thresholding. Using the conditions given in Table 2, the urban, vegetation, greenhouse and water areas were determined for the years 2004, 2009, 2013, 2017 and 2021. Finally, the areas and area changes of land cover classes from 2004 to 2021 were calculated.

Index	Formulation	Reference
NDVI	(Nir-R)/(Nir+R)	Rouse et al., 1973
NBRT	((Nir-Swir1*(Thermal/100))/ (Nir+Swir1*(Thermal/100)))	Holden et al., 2005
MNDWI	(G-Swir)/(G+Swir)	Xu, 2006
IBI	(2*Swir1/(Swir1+Nir)-(Nir/(Nir+R)+G/(G+Swir1)))/ (2*Swir1/(Swir1+Nir)-(Nir/(Nir+R)+G/(G+Swir1)	Xu, 2008
PMLI	(Swir1-R)/(Swir1+R)	Lu et al., 2014
PGI	100* ((B*(Nir-R))/ (1-((B+G+R)/3)))	Yang et al., 2017
MBI	((Swir1- Swir2-Nir)/ (Swir1+Swir2+Nir))+f (f is additional factor; f = 0.5)	Nguyen et al., 2021
where	B = Blue band (0.45-0.51μm), G = Green band (0.53-0.59μm), R = Red band (0.64-0.67μm), Nir = Near infrared band (0.85-0.88μm), Swir1 = Short-wave infrared band (1.57-1.65μm), Swir2 = Short-wave infrared (2.11-2.29μm).	

Table 1. The land cover indices used in this study and their formulations.

Land Cover	Threshold Conditions
Urban	$IBI > IBI_{thr1}$ & $MBI > MBI_{thr1}$
Vegetation	$NDVI > NDVI_{thr2}$
Water	$MNDWI > MNDWI_{thr}$
Greenhouse	$PGI > PGI_{thr}$ & $IBI < IBI_{thr2}$ & $MBI > MBI_{thr1}$ (*Landsat 5 TM*)
	$PMLI < PMLI_{thr}$ (*Landsat 8 OLI/TIRS*)
Burned	$NBRT < NBRT_{thr1}$

Table 2. The usage of automatically determined threshold values to detect land cover classes.

3.2 Generation of LST Maps

Various methods are available to obtain LST values from Landsat thermal band/bands. The Landsat 5 TM satellite has a single thermal band. Thus, in this study, a method that uses a single thermal band and does not require atmospheric parameters is preferred (Artis and Carnahan, 1982; Weng et al, 2004). The LST values were calculated using the 6th band of the Landsat 5 TM the and the 10th band of the Landsat 8 OLI/TIRS imageries and emissivity data created from the NDVI. The brightness temperature data were obtained with the formulas on the USGS website (USGS, 2021).

Firstly, Landsat thermal DN values were converted to Top of Atmosphere (TOA) spectral radiance using the spectral constants in the Metadata file:

$$L_\lambda = M_L * Q_{cal} + A_L \quad (1)$$

where L_λ = TOA spectral radiance (Watts/(m^2 * srad *μm)),
M_L = Band-specific multiplicative rescaling factor from the metadata file,
A_L = Band-specific additive rescaling factor from the metadata file,
Q_{cal} = Quantized and calibrated standard pixel values.

Then, brightness temperature values were calculated from the spectral radiance values:

$$T_B = K_2 / \ln(K_1 / L_\lambda + 1) \quad (2)$$

where T_B = TOA brightness temperature (K),
K_1 and K_2 are band-specific thermal conversion constants from the metadata file.

Finally, LST values were determined with the NDVI threshold method (Sobrino et al., 2004 and Sobrino et al, 2008) and the emissivity corrected LST values were calculated (Artis and Carnahan, 1982; Weng et al, 2004).

$$LST = T_B / (1 + (\lambda * T_B / \alpha) * \ln\varepsilon) \quad (3)$$

where λ = average wavelength of the thermal band
$\alpha = 1.438 * 10^{-2}$ mK,
ε = emissivity value (Sobrino et al., 2004 and Sobrino et al, 2008).

$$\varepsilon\lambda = \begin{cases} \varepsilon_{s\lambda} & NDVI < NDVI_S \\ \varepsilon_{s\lambda} + (\varepsilon_{v\lambda} - \varepsilon_{s\lambda}) * P_V & NDVI_S \le NDVI \le NDVI_V \\ \varepsilon_{v\lambda} & NDVI > NDVI_V \end{cases} \quad (4)$$

where $\varepsilon_{s\lambda}$ = 0.980-0.042*R (R is the reflectance values of Red Band)
$\varepsilon_{v\lambda}$ = 0.99
$NDVI_S$ = 0.2 and
$NDVI_V$ = 0.5 (Sobrino et al., 2008).
P_V (Carlson and Ripley, 1997) is vegetation proportion and its calculated using the equation 5.

$$P_V = (NDVI-NDVI_S)/(NDVI_V-NDVI_S)^2 \quad (5)$$

3.3 Accuracy Assessment of Land Cover Classification and LST Determination

Confusion matrix is a frequently and effectively used accuracy assessment technique to evaluate the performance of classification accuracy (Congalton, 1991; Koc-San and Sonmez, 2016). It is a good rule of thumb to collect at least 50 samples for each land cover category in the error matrix unless the area is very large and there are not many (i.e., less than 12 categories) land cover class (Congalton, 1991). In this study, to determine the accuracy of the land cover maps, 500 test pixels for each area were collected and error matrices were created. In this way, Producer's Accuracy (PA), User's Accuracy (UA), Overall Accuracy (OA), and Kappa Coefficient (KC) values were calculated for the years 2004, 2009, 2013, 2017, 2021 and given in Tables 3, 4, 5, 6, 7, respectively.

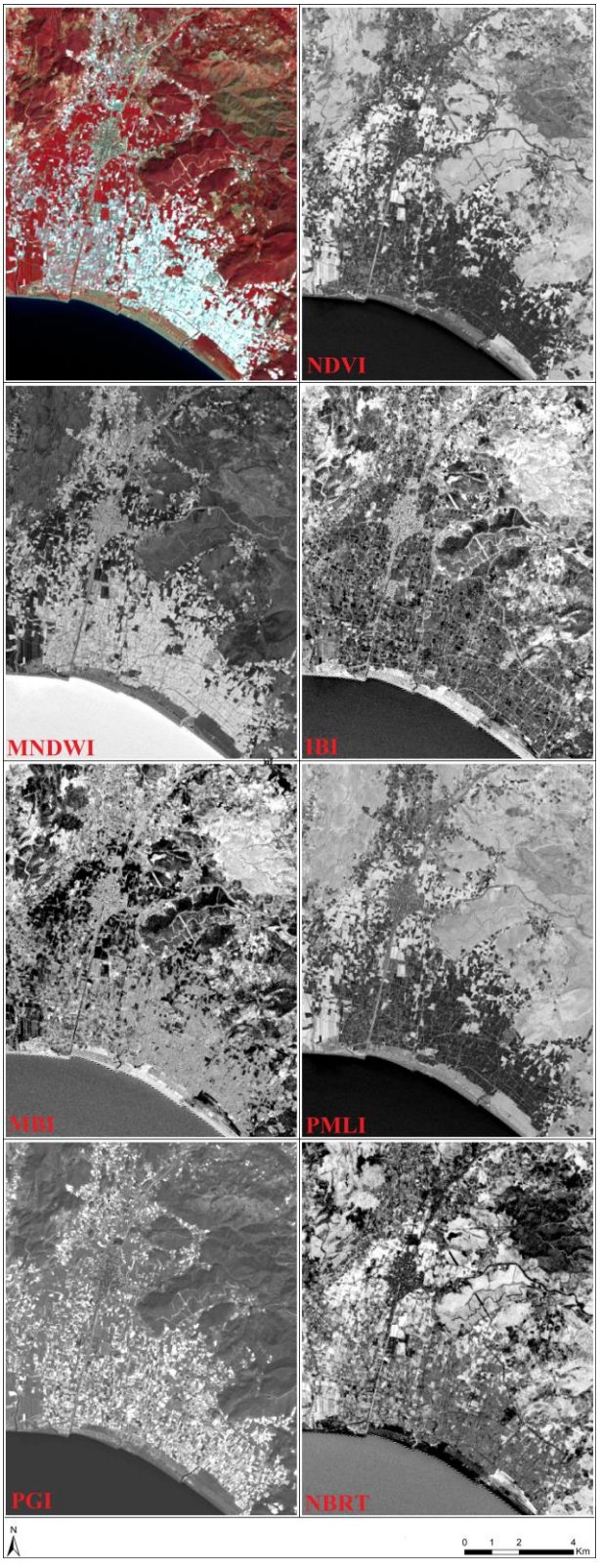

Figure 2. The false colour composite image and the obtained land cover indices of the study area for the year 2021.

		Test Data				
Land Cover Class	U	V	G	W	Bl	
Urban (U)	302	0	12	0	0	
Vegetation (V)	24	496	10	0	17	
Greenhouse (G)	61	0	202	0	63	
Water (W)	0	0	0	500	0	
Bareland (Bl)	113	4	276	0	420	
PA	0.60	0.99	0.40	1.00	0.84	
UA	0.96	0.90	0.61	1.00	0.51	
OA: 0.76;	KC: 0.71					

Table 3. The confusion matrix of land cover classes for 2004.

		Test Data				
Land Cover Class	U	V	G	W	Bl	
Urban (U)	317	0	12	0	0	
Vegetation (V)	1	500	20	0	17	
Greenhouse (G)	30	0	199	0	5	
Water (W)	0	0	0	500	0	
Bareland (Bl)	152	0	266	0	478	
PA	0.63	1.00	0.40	1.00	0.95	
UA	0.96	0.92	0.85	1.00	0.53	
OA: 0.79	KC: 0.74					

Table 4. The confusion matrix of land cover classes for 2009.

		Test Data					
Land Cover Class	U	V	G	B	W	Bl	
Urban (U)	334	0	12	0	1	4	
Vegetation (V)	0	500	28	3	0	0	
Greenhouse (G)	73	0	335	0	0	3	
Burned (B)	0	0	0	215	0	63	
Water (W)	0	0	0	0	499	0	
Bareland (Bl)	92	0	125	196	0	430	
PA	0.66	1.00	0.67	0.52	0.99	0.86	
UA	0.95	0.94	0.81	0.77	1.00	1.00	
OA: 0.79	KC: 0.75						

Table 5. The confusion matrix of land cover classes for 2013.

		Test Data					
Land Cover Class	U	V	G	B	W	Bl	
Urban (U)	376	0	33	0	0	2	
Vegetation (V)	2	499	3	0	0	0	
Greenhouse (G)	83	0	436	0	0	90	
Burned (B)	0	0	0	482	0	23	
Water (W)	0	0	0	0	500	0	
Bareland (Bl)	39	1	28	18	0	385	
PA	0.75	0.99	0.87	0.96	1.00	0.77	
UA	0.91	0.99	0.71	0.95	1.00	0.81	
OA: 0.89	KC: 0.87						

Table 6. The confusion matrix of land cover classes for 2017.

		Test Data					
Land Cover Class	U	V	G	B	W	Bl	
Urban (U)	388	0	36	0	0	7	
Vegetation (V)	0	490	0	0	0	4	
Greenhouse (G)	72	3	427	3	0	23	
Burned (B)	0	0	0	337	0	17	
Water (W)	0	0	0	0	500	0	
Bareland (Bl)	40	7	37	160	0	449	
PA	0.77	0.98	0.85	0.67	1.00	0.89	
UA	0.90	0.99	0.81	0.95	1.00	1.00	
OA: 0.86	KC: 0.83						

Table 7. The confusion matrix of land cover classes for 2021.

In this study, the validity of obtained LST values was evaluated by examining their relationship with MODIS LST data. MODIS LST/Emissivity data was converted to LST values using the (0.02) rescaling factor (Wan, 2021). Landsat and MODIS LST correlation values were obtained higher than 0,80.

4. RESULTS AND DISCUSSION

In this study, the land cover and LST changes of Kumluca district were investigated from 2004 to 2021. When the error matrices are examined, generally it can be said that the land covers can be mapped quickly and effectively using indices and automatic thresholding values. Using this method, it is seen that the land cover classification can be obtained with overall accuracy values higher than 76% and kappa coefficient values higher than 0.71. The classes with the highest classification accuracy were, as expected, water and vegetation. These areas were classified almost completely correctly. On the other hand, the obtained results indicate that the accuracies of urban and greenhouse areas are relatively lower from the other classes, especially for the years that Landsat 5 used. Figure 3 shows the infrared colour composite study area image and produced land cover and land surface temperature maps for the years 2004, 2009, 2013, 2017 and 2021.

4.1 Land Cover Classification and Land Cover Changes from 2004 to 2021

The calculated land cover areas for the years 2004, 2009, 2013, 2017 and 2021 were given in Table 8. The urban area, which was approximately 4.40 km^2 in 2004, has increased continuously and reached to 8.89 km^2 in 2021. Likewise, greenhouse areas, which were 15.47 km^2 in 2004, increased to 33.45 km^2 by the year 2021. The Mediterranean Sea is in the south of the study area and, as expected, no change was observed for water class (17.19 km^2) in the study area. Vegetation areas decreased from 67.82 km^2 to 51.10 km^2 from 2004 to 2021. A major fire broke out in 2016 and damaged significant amount of the vegetation areas in the study area. Also, the burned area is visible in the 2013 image. Therefore, in 2013, 2017 and 2021, the images were classified as urban, vegetation, greenhouse, burned, water and bareland areas. The burned areas were 2.71 km^2 in 2013. After the fire in 2016, the burned areas increased to 12.53 km^2 in 2017, then decreased to 6.48 km^2 in 2021. Although the burned areas started to be covered with vegetation again, approximately 6.48 km^2 burned area detected in 2021. Mountainous, sand, vacant areas were classified as bareland areas. The bareland areas were decreased from 41.40 km^2 in 2004 to 39.82 km^2, 37.95 km^2 and 27.09 km^2 in 2009, 2013 and 2017, respectively. In 2021 the bareland areas decreased to 29.17 km^2.

Area (km^2)	2004	2009	2013	2017	2021
Urban	4.40	4.51	6.96	7.65	8.89
Vegetation	67.82	69.20	64.85	52.45	51.10
Greenhouse	15.47	15.60	16.66	29.41	33.45
Water	17.19	17.19	17.19	17.19	17.19
Burned	-	-	2.71	12.53	6.48
Bareland	41.40	39.82	37.95	27.09	29.17

Table 8. Land cover areas (km^2) from 2004 to 2021.

The percentage of urban, vegetation, greenhouse, water, burned and bareland areas in the total area in 2004 and 2021 and their changes in this period are shown in Table 9. While vegetation areas constituted approximately 46.36% of the total area in 2004, it decreased by the year 2021 to 34.93%. It is the bareland class of area with the highest share with 28.30% after vegetation areas. In this class, it decreased by 12.23 km^2 from 2004 to 2021 and its share in the area decreased to 19.94%. On the other hand, urban and greenhouse areas have increased over the years. Greenhouse areas increased by 17.98 km^2 and its share in the study area increased from 10.58% to 22.87%.

Percentage(%)	2004(%)	2021(%)	Δ(%)	Δ(km^2)
Urban	3.01	6.08	3.07	4.49
Vegetation	46.36	34.93	-11.43	-16.72
Greenhouse	10.58	22.87	12.29	17.98
Water	11.75	11.75	0.00	0.00
Burned	0.00	4.43	4.43	6.48
Bareland	28.30	19.94	-8.36	-12.23

Table 9. Percentages of land cover classes in 2004 and 2021 and their changes in 17 years.

The change matrix of land cover areas was created for the years 2004 and 2021 and it is given in Table 10. Looking at the change matrix, it can be said that the greenhouse, burned and urban areas were increased in Kumluca from 2004 to 2021. On the other hand, the vegetation and bareland areas decreased in the same time period. When the change matrix is examined, it is seen that some urban, vegetation and bareland areas had turned into greenhouse areas in 2021. The classes that most transform into greenhouse area are vegetation and bareland areas. 6.44 km^2 of vegetation areas had been transformed into greenhouse areas. Additionally, 15.50 km^2 of the bareland areas, which corresponds to approximately 1/3 of the area, has been transformed into a greenhouse area. However, 3.66 km^2 of vegetation was destroyed and turned into a burned area in 2021.

	2021						2004
2004	U	V	G	W	B	Bl	Total
U	3.39	0.08	0.48	0.00	0.00	0.45	4.40
V	2.51	43.61	6.44	0.00	3.66	11.60	67.82
G	2.01	0.68	11.03	0.00	0.00	1.75	15.47
W	0.00	0.00	0.00	17.19	0.00	0.00	17.19
B	0.00	0.00	0.00	0.00	0.00	0.00	0.00
Bl	0.98	6.73	15.50	0.00	2.82	15.37	41.40
2021 Total	8.89	51.10	33.45	17.19	6.48	29.17	146.28
C.C.	4.49	-16.72	17.98	0.00	6.48	-12.23	

Table 10. Change detection matrix of land cover from 2004 to 2021 in km^2. (Urban-U; Vegetation-V; Greenhouse-G; Water-W; Burned-B; Bareland-Bl; Class Change-C.C.)

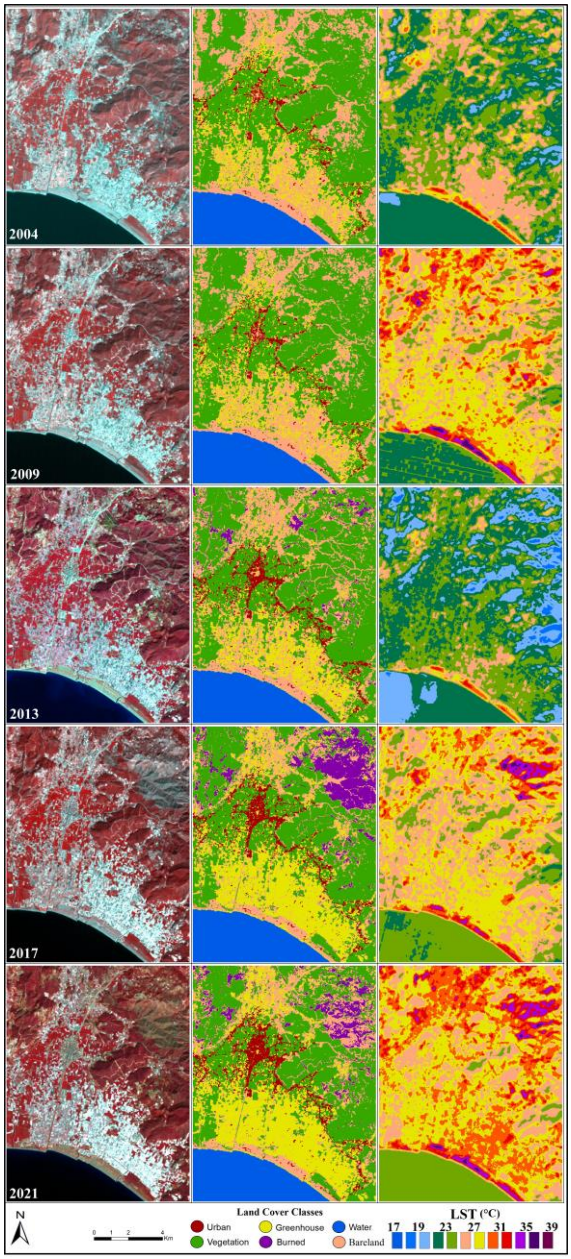

Figure 3. Different views of study area for the years. (left) the infrared colour composites, (middle) land cover classes and (right) LST images of the study area.

4.2 LST Values and Their Changes from 2004 to 2021

The LST values of the land cover classes are shown in Table 11. LST values of all classes increased in 2004 to 2021. The LST increase for urban, vegetation, greenhouse, water, and bareland areas are 3.99°C, 4.30°C, 3.95°C, 2.29°C and 4.16°C, respectively. In this study, the 2013 was the year with the lowest temperatures of all land classes.

LST (°C)	2004	2009	2013	2017	2021
Urban	25.92	29.53	24.61	28.48	29.91
Vegetation	23.96	27.64	22.59	26.96	28.26
Greenhouse	26.13	29.08	25.65	28.80	30.08
Water	22.90	24.02	22.08	24.24	25.19
Burned	-	-	25.76	31.02	32.79
Bareland	26.72	30.24	25.03	29.35	30.88
$SUHI_{urb-water}$	3.02	5.51	2.53	4.24	4.72

Table 11. LST values for the years 2004, 2009, 2013, 2017 and 2021.

The highest temperature increase was observed in the vegetation land cover areas with 4.30°C. It is thought that this situation may be caused by the areas damaged in the fire and covered with vegetation again. The other area, where the temperature increased mostly is the bareland areas with 4.16°C in the same period. The least temperature increase was observed for the water areas with 2.29°C from 2004 to 2021. The temperature increase in urban and greenhouse areas was determined about 4.00°C, which is quite high. Generally, the LST values of greenhouses were slightly higher than urban areas but lower than bareland areas.

When the LST changes between 2013-2021 are examined, the land cover type with the highest LST values is the burned areas with 7.03°C. These areas are followed by barelands, vegetation, urban, greenhouse and water areas with 5.85°C, 5.67°C, 5.30°C, 4.43°C and 3.11°C, respectively.

Figure 4 shows the relationship between land cover type change and LST change. The highest temperature increase in the study period was 9.0°C degrees in the areas which change from vegetation into burned areas. These areas are followed by the areas that changed from vegetation to bareland with 5.9°C and from vegetation to urban with 4.9°C and vegetation to greenhouse with 4.9°C.

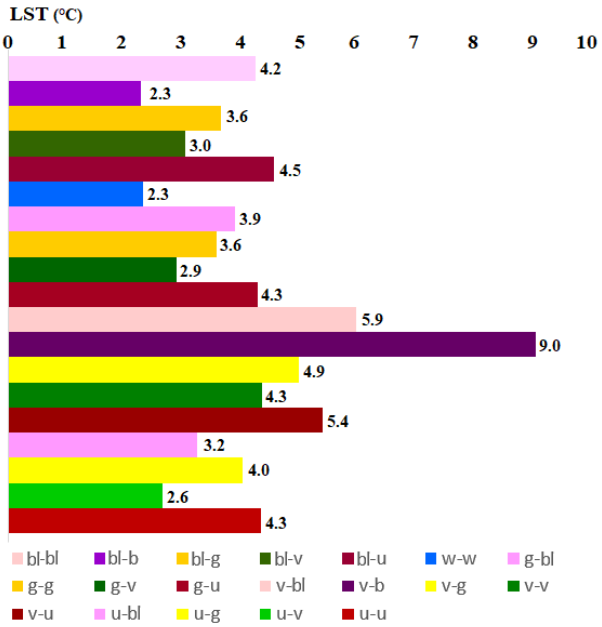

Figure. 4. Graph of the relationship between land cover type change and LST change (bl: bareland, b: burned, g: greenhouse, v: vegetation, u: urban and w: water areas).

The phenomenon of urban that have different surface properties compared to the natural/rural areas around them being warmer than their surrounding surfaces is called the Surface Urban Heat Island (SUHI) effect. While examining this situation, the difference between urban and water LST values can be used (Chen et al., 2006). Hence, in this study for computing the SUHI effect the LST differences between urban and water areas in the study area were calculated. While this difference was highest with 5.51℃ in 2009, and 4.72℃ in 2021, calculated lowest in 2013 with 2.53℃. Moreover, the $SUHI_{urban\text{-}water}$ magnitudes, which was 3.02℃ in 2004, increased to 4.24℃ in 2017 and 4.72℃ in 2021.

5. CONCLUSIONS

Türkiye is among the top four countries in the world in terms of greenhouse production, and 3.8 million tons production, which is 48% of greenhouse production, is made in Antalya. Kumluca district of Antalya is one of the important centres of greenhouse production with its many plastic-covered greenhouse areas. This situation has an impact on the land cover change of Kumluca. Using NDVI, MNDWI, IBI, MBI, PMLI, PGI and NBRT indices, land cover areas could be determined with an overall accuracy of over 76%. As expected, water and vegetation areas were determined with high accuracy. However, it has been observed that urban areas can be mixed with greenhouse areas. In this paper, a useful and effective approach to address the processes of land cover mapping was presented for Kumluca.

It was observed that urban and greenhouse areas increased in Kumluca from 2004 until 2021. It was also determined that vegetation and bareland areas decreased. It is seen that there is a change from barelands and vegetation areas into the greenhouse areas from 2004 to 2021. In addition, some of the barelands changed as urban areas within this time period. It was also observed that the LST values increased almost for all land cover classes from 2004 to 2021.

As a result, the approach applied in this study can provide effective and accurate land cover and LST maps in areas that do not contain complex land classes, such as Kumluca.

REFERENCES

Artis, D.A., Carnahan, W.H., 1982. Survey of emissivity variability in thermography of urban areas. *Remote Sens Environ*, 12, 313–329.

Aslan, N., Koc-San, D., 2021. The Use of Land Cover Indices for Rapid Surface Urban Heat Island Detection from Multi-Temporal Landsat Imageries. *ISPRS Int. J. Geo-Inf*, 10, 416.

Carlson, T.N., Ripley, D.A. 1997. On the relation between NDVI, fractional vegetation cover, and leaf area index. *Remote Sens. Environ.* 62, 241–252.

Chen, X.L.; Zhao, H.M.; Li, P.X.; Yin, Z.Y., 2006. Remote sensing image-based analysis of the relationship between urban heat island and land use/cover changes. *Remote Sens. Environ.*, 104, 133–146.

Congalton, R.G., 1991. A review of assessing the accuracy of classifications of remotely sensed data. *Remote Sens. Environ.*, 37, 35–46.

Estoque, R.C., Murayama, Y., Myint, S.W., 2017. Effects of landscape composition and pattern on land surface temperature: An urban heat island study in the megacities of Southeast Asia. *Sci. Total Environ*., 577, 349–359.

González-Yebra, Ó., Aguilar, M. A., Nemmaoui, A., Aguilar, F. J., 2018. Methodological proposal to assess plastic greenhouses land cover change from the combination of archival aerial orthoimages and Landsat data. *Biosystems Engineering*, 175, 36-51.

Holden, Z.A., Smith, A.M.S., Morgan, P., Rollins, M.G., Gessler, P.E., 2005. Evaluation of novel thermally enhanced spectral indices for mapping fire perimeters and comparisons with fire atlas data. *International Journal of Remote Sensing* (26), 21, 4801-4808.

Koc-San, D., Sonmez, N. K., 2016: Plastic and Glass Greenhouses Detection and Delineation from Worldview-2 Satellite Imagery, Int. Arch. Photogramm. Remote Sens. Spatial Inf. Sci., XLI-B7, 257–262, https://doi.org/10.5194/isprs-archives-XLI-B7-257-2016.

Lu, L., Di, L., Ye, Y., 2014. A decision-tree classifier for extracting transparent plastic-mulched landcover from Landsat-5 TM images. *IEEE Journal of Selected Topics in Applied Earth Observations and Remote Sensing*, 7(11), 4548e4558.

Mathew, A., Khandelwal, S., Kaul, N, 2017. Investigating spatial and seasonal variations of urban heat island effect over Jaipur city and its relationship with vegetation, urbanization and elevation parameters. *Sustain. Cities Soc.*, 35, 157–177.

Muzaky, H., Jaelani, L.M., 2019. Analysis of the impact of land cover on Surface Temperature Distribution: Urban heat island studies i}n Medan and Makassar. *IOP Conf. Ser. Earth Environ. Sci*., 389, 012047.

Nega, W., Balew, A., 2022. The relationship between land use land cover and land surface temperature using remote sensing: systematic reviews of studies globally over the past 5 years. *Environmental Science and Pollution Research*, https://doi.org/10.1007/s11356-022-19997-z.

Nguyen, C.T., Chidthaisong, A., Diem, P.K., Huo, L.Z., 2021. A Modified Bare Soil Index to Identify Bare Land Features during Agricultural Fallow-Period in Southeast Asia Using Landsat 8. *Land*, 10, 231. https://doi.org/10.3390/land10030231.

Otsu, N.A, 1979. Threshold Selection Method from Gray-Level Histograms. *IEEE Trans. Syst. Man Cybern*, 9, 62–66.

Pal, S., Ziaul, S, 2017. Detection of land use and land cover change and land surface temperature in English Bazar urban centre. *Egypt. J. Remote Sens. Sp. Sci.*, 20, 125–145.

Republic of Türkiye Ministry of Agriculture and Forestry. 2023: The current situation in our greenhouse and greenhouse production. https://www.tarimorman.gov.tr/Konular/Bitkisel-Uretim/Tarla-Ve-Bahce-Bitkileri/Ortu-Alti-Yetistiricilik (accessed 10.07.2023).

Rouse, J.W., Haas, R.H., Schell, J.A., Deering, D.W., 1974: Monitoring Vegetation Systems in the Great Plains with ERTS.

In Proceedings of the Third Earth Resources Technology Satellite-1 Symposium, Greenbelt, MD, USA, 10–14 December 1973. NASA SP-351 Series.

Salas, E.A.L., Henebry, G.M., 2012. Separability of maize and soybean in the spectral regions of chlorophyll and carotenoids using the moment distance index. *Israel Journal of Plant Science*, 60(1-2), 65-76.

Sekertekin, A., Kutoglu, S.H., Kaya, S., 2016. Evaluation of spatio-temporal variability in Land Surface Temperature: A case study of Zonguldak, Turkey. *Environmental monitoring and assessment*, 188, pp. 1-15.

Sekertekin, A.; Zadbagher, E, 2021. Simulation of future land surface temperature distribution and evaluating surface urban heat island based on impervious surface area. *Ecol. Indic*., 122, 107230.

Singh, P., Kikon, N., Verma, P, 2017. Impact of land use change and urbanization on urban heat island in Lucknow city, Central India. A remote sensing based estimate. *Sustain. Cities Soc.*, 32, 100–114.

Sobrino, J.A., Jiménez-Muñoz, J.C. Paolini, L., 2004. Land surface temperature retrieval from LANDSAT TM 5. *Remote Sens Environ*, 90, 434–440.

Sobrino, J.A., Jiménez-Muñoz, J.C., Sòria, G.; Romaguera, M.; Guanter, L.; Moreno, J.; Plaza, A.; Martínez, P., 2008. Land surface emissivity retrieval from different VNIR and TIR sensors. *IEEE Trans. Geosci. Remote Sens*., 46, 316–327.

Tan, J., Yu, D., Li, Q., Tan, X., Zhou, W., 2020. Spatial relationship between land-use/land-cover change and land surface temperature in the Dongting Lake area, China. *Scientific reports*, 10: 9245, https://doi.org/10.1038/s41598-020-66168-6.

Wan, Z. 2013. Collection-6 MODIS Land Surface Temperature Products Users' Guide. Available online: https://lpdaac.usgs.gov/documents/118/MOD11_User_Guide_V6.pdf (accessed on 18 January 2021).

Weng, Q., Lu, D.; Schubring, J., 2004. Estimation of land surface temperature-vegetation abundance relationship for urban heat island studies. *Remote Sens. Environ*., 89, 467–483.

USGS, 2021: Using the USGS Landsat Level-1 Data Product. https://www.usgs.gov/core-science-systems/nli/landsat/using-usgs-landsat-level-1-data-product (accessed on 29 January 2022).

Xu, H., 2006. Modification of normalised difference water index (NDWI) to enhance open water features in remotely sensed imagery. *Int. J. Remote Sens.*, 27, 3025–3033.

Xu, H. 2008. A new index for delineating built-up land features in satellite imagery. Int. J. Remote Sens. 29, 4269–4276.

Yang, D., Chen, J., Zhou, Y., Chen, X., Chen, X., Cao, X., 2017. Mapping plastic greenhouse with medium spatial resolution satellite data: Development of a new spectral index. *ISPRS J. Photogramm. Remote Sens*., 128, 47–60.

Zhao, M., Cai, H., Qiao, Z., Xu, X, 2016. Influence of urban expansion on the urban heat island effect in Shanghai. *Int. J. Geogr. Inf. Sci*., 30, 2421–2441.